Optics Letters

Femtosecond-laser-written Tm:KLu$(WO_4)_2$ waveguide lasers

Esrom Kifle,[1] Xavier Mateos,[1,2,*] Javier Rodríguez Vázquez de Aldana,[3] Airan Ródenas,[1,4] Pavel Loiko,[5] Sun Yung Choi,[6] Fabian Rotermund,[7] Uwe Griebner,[2] Valentin Petrov,[2] Magdalena Aguiló,[1] and Francesc Díaz[1]

[1]Física i Cristal·lografia de Materials i Nanomaterials (FiCMA-FiCNA), Universitat Rovira i Virgili (URV), Campus Sescelades, c/Marcel·lí Domingo, s/n., E-43007 Tarragona, Spain
[2]Max Born Institute for Nonlinear Optics and Short Pulse Spectroscopy, Max-Born-Str. 2a, D-12489 Berlin, Germany
[3]Aplicaciones del Láser y Fotónica, University of Salamanca, 37008 Salamanca, Spain
[4]Istituto di Fotonica e Nanotecnologie-Consiglio Nazionale delle Ricerche (IFN-CNR), Piazza Leonardo da Vinci, 32, I-20133 Milano, Italy
[5]ITMO University, 49 Kronverkskiy pr., 197101, St. Petersburg, Russia
[6]Department of Energy Systems Research, Ajou University, 16499 Suwon, South Korea
[7]Department of Physics, KAIST, 291 Daehak-ro, Yuseong-gu, 34141 Daejeon, South Korea
*Corresponding author: xavier.mateos@urv.cat

Received 12 December 2016; revised 28 January 2017; accepted 2 February 2017; posted 24 February 2017 (Doc. ID 282633); published 14 March 2017

Depressed-index channel waveguides with a circular and photonic crystal cladding structures are prepared in a bulk monoclinic Tm:KLu$(WO_4)_2$ crystal by 3D direct femtosecond laser writing. The channel waveguide structures are characterized and laser operation is achieved using external mirrors. In the continuous-wave mode, the maximum output power of 46 mW is achieved at 1912 nm corresponding to a slope efficiency of 15.2% and a laser threshold of only 21 mW. Passive *Q*-switching of a waveguide with a circular cladding is realized using single-walled carbon nanotubes. Stable 7 nJ/50 ns pulses are achieved at a repetition rate of 1.48 MHz. This first demonstration of ~2 μm fs-laser-written waveguide lasers based on monoclinic double tungstates is promising for further lasers of this type doped with Tm^{3+} and Ho^{3+} ions.

OCIS codes: (230.7380) Waveguides, channeled; (140.3540) Lasers, Q-switched; (140.3380) Laser materials.

https://doi.org/10.1364/OL.42.001169

During the past decade, femtosecond-laser direct-written (fs-DLW) waveguides in transparent amorphous and crystalline materials have emerged as an enabling technology for the production of passive and laser-active integrated photonic devices [1–3]. DLW offers localized and permanent refractive index variation [2,3], short interaction time, and high precision of the process preserving high optical quality of the core. As a result, efficient and power-scalable laser operation with rare-earth-doped fs-DLW waveguides is possible. With Yb^{3+} [4,5] and Nd^{3+} [6–9] ions at ~1 μm, fs-DLW waveguide lasers with a nearly quantum-defect-limited efficiency and multi-watt output have been realized.

Thulium (Tm^{3+}) ions are known for their eye-safe broadband emission at ~2 μm (the $^3F_4 \rightarrow {}^3H_6$ transition). This is in the specific spectral range where absorption lines of relevant molecules, e.g., H_2O and CO_2, are located. Tm lasers and, in particular, Tm waveguide lasers are thus interesting for environmental and medical sensing applications. To date, fs-DLW Tm waveguide lasers in glasses (e.g., ZBLAN) [10,11] and cubic crystals (YAG) [12] have been reported. In particular, a fs-DLW Tm:ZBLAN laser generated 205 mW at 1.89 μm with a slope efficiency of 67% [11].

Monoclinic double tungstates (DTs), KRE$(WO_4)_2$ where RE = Gd, Y, or Lu, doped with Tm^{3+} ions, are known as excellent materials for bulk [13] and liquid-phase epitaxy grown waveguide lasers [14] at ~2 μm owing to high transition cross sections and broad spectral bands of Tm^{3+} ions [15]. In addition, Tm:DTs offer the possibility of high doping levels together with a weak concentration quenching and a strong cross-relaxation (CR) mechanism that results in a quantum efficiency of almost two [16]. Efficient and compact Tm:DT lasers based on thermal- and index-guiding were already demonstrated [16,17].

In the present work, the first fs-DLW Tm:DT waveguide laser is realized (fs-DLW lasers based on Yb:DTs have been studied before [18]). It is based on Tm:KLu$(WO_4)_2$ (Tm:KLuW) as an active material and operates both in the continuous-wave (CW) and passively *Q*-switched (PQS) mode. In the latter case, we employed single-walled carbon nanotubes (SWCNTs) as a saturable absorber, SA, a material whose ultrafast and broadband saturable absorption properties [19] have been widely exploited in pulsed near-IR lasers. SWCNTs have been used before in a PQS microchip Tm:KLuW laser resulting in record short pulse durations [20].

Depressed-index waveguides were fabricated in a bulk Tm:KLuW crystal by 3D ultrafast fs-pulse laser direct writing. The

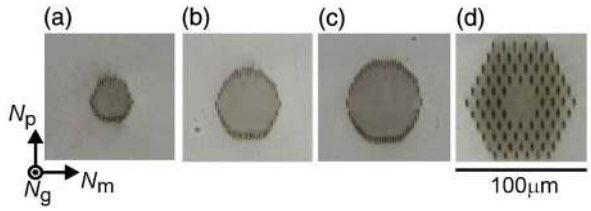

Fig. 1. Bright-field microscope images of the facet cross section of the fs-DLW channel waveguides W1–W4 (a)–(d) in Tm:KLuW.

crystal was grown by the top-seeded-solution growth method. It was doped with 3 at. % Tm^{3+} ($N_{Tm} = 2.15 \times 10^{20}$ at/cm^3. A rectangular sample was cut from this crystal along the N_g-axis [length: 2.96 mm, aperture: 3.10(N_m)× 2.85(N_p) mm^2], both $N_m \times N_p$ faces were polished to laser quality. Two types of cladding waveguides were prepared, namely exhibiting circular cladding with diameters of 30 μm (W1), 40 μm (W2) and 50 μm (W3), or having a photonic-crystal-like cladding with a core diameter of 30 μm (W4), see Fig. 1. All waveguides were written by employing 120 fs, 795 nm pulses from a Ti:sapphire regenerative amplifier (Spitfire, Spectra Physics) employing only a small fraction of the output energy at a repetition rate of 1 kHz. The laser beam was focused with a 40 × microscope objective (NA = 0.65). The incident pulse energy on the crystal was set to 57 nJ (for W1–W3) or 73 nJ (W4), with the help of a half-wave plate, a linear polarizer, and a calibrated neutral density filter. The sample was scanned at a constant speed of 400 μm/s (for W1–W3) or 300 μm/s (W4) along the N_g-axis of the crystal thus producing damage tracks. The polarization of the fs laser was perpendicular to the scanning direction ($E \| N_m$) thus avoiding anisotropic effects related to the birefringence of DTs. The line scan procedure was repeated consecutively at different depths and lateral positions of the sample, following the desired geometry. The axis of the waveguides was located at 120 μm beneath the crystal surface. The lateral separation between each two adjacent tracks was 2 μm (for W1–W3) or 8 μm (W4).

To characterize the modification of the crystal structure in the core and cladding of the micro-fabricated waveguides, a micro-Raman analysis was performed. A Renishaw inVia Reflex microscope equipped with a 514 nm argon laser and a 50 × Leica objective was used. The facet cross section of the waveguides was studied with a spatial resolution of 0.4 μm, Fig. 2. The polarization of the excitation laser corresponded to $E \| N_m$. The most intense ~907 cm^{-1} stretching phonon mode, assigned as $\nu(W-O)/\nu_1$ [13], was analyzed; its peak position, full width at half-maximum (FWHM), and peak intensity were monitored. In the core region, the crystalline quality of the material is fully preserved, a feature that allows developing integrated lasers. The cladding region consists of slightly damaged material, as indicated by the decrease of intensity and broadening of the phonon mode, Figs. 2(b) and 2(c). The existence of a residual anisotropic stress field is also evidenced by the phonon energy shifts outside the cladding volume, Fig. 2(a). These stress fields further create a birefringence effect and favor the polarization-selective response of the waveguide [21].

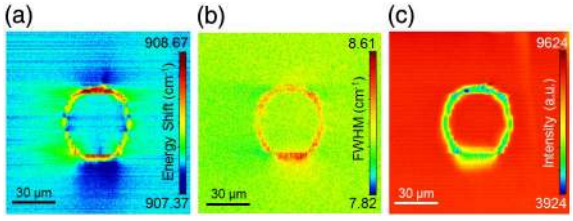

Fig. 2. Micro-Raman mapping of the facet cross section of the fs-DLW circular-cladding Tm:KLuW waveguide (W2) measuring the high gain 907 cm^{-1} phonon mode: (a) phonon energy shift, (b) full width at half-maximum, and (c) peak intensity.

The Tm:KLuW sample containing the four fs-DLW waveguides was placed on a passively cooled glass substrate. The laser cavity consisted of a flat pump mirror (PM) that was antireflection coated for 0.7–1 μm and high-reflection coated for 1.8–2.1 μm and a flat output coupler (OC) providing a transmission of $T_{OC} = 3\%$, 5%, or 9% at 1.8–2.1 μm. Both the PM and OC were placed as close as possible to the faces of the sample without the use of index-matching liquid to avoid laser-induced damage of the faces. As a pump source, we used a CW Ti:sapphire laser (Coherent, Model MIRA 900) tuned to 802 nm ($^3H_6 \rightarrow {}^3H_4$ transition of the Tm^{3+} ion). The polarization of the pump beam corresponded to $E \| N_m$ in Tm:KLuW. The pump light was coupled into the waveguide with a 10 × microscope objective lens (NA: 0.28, focal length: 20 mm). The incident pump power was varied with a gradient neutral density filter placed in front of the objective. The pump beam radius in the focus was ~20 μm. The pump absorption under lasing conditions (~75%) was determined by a combination of the waveguide propagation experiment (at 830 nm), the pump-absorption one (at 802 nm), and a rate-equation modeling. In this way, the pump coupling efficiency was taken into account.

The output characteristics of the W1–W4 waveguide lasers are presented in Fig. 3(a) for $T_{OC} = 9\%$. In all cases the laser output was linearly polarized, $E \| N_m$. The best performance was observed for the W2 waveguide. This waveguide laser generated 46 mW at 1.912 μm corresponding to a slope efficiency η of 15.2% (with respect to the absorbed pump power). The laser threshold was at $P_{abs} = 21$ mW. For the W1, W3, and W4 waveguide devices, the laser performance was inferior. The laser performance of the W2 waveguide for different OCs is shown in Fig. 3(b). The measured η is limited by the losses at the crystal–mirror interfaces, non-optimized pump coupling,

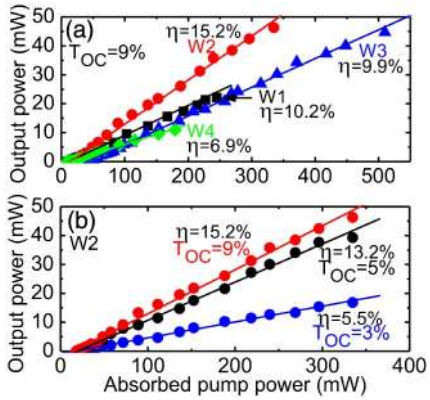

Fig. 3. Output power of the CW fs-DLW Tm:KLuW waveguide lasers: (a) W1–W4 waveguides for $T_{OC} = 9\%$, (b) W2 waveguide for various OCs, η-slope efficiency.

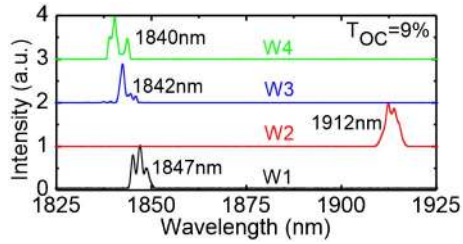

Fig. 4. Typical CW laser emission spectra of the fs-DLW Tm:KLuW waveguide lasers, at maximum P_{abs} according to Fig. 3(a).

and relatively low T_{OC} used (for waveguide lasers). During CW laser operation, no thermally induced cracks or damage of the material were observed.

The propagation losses in the fs-DLW Tm:KLuW waveguides were estimated with the Caird analysis as ~1.4 ± 0.5 dB/cm (a mean value for the W1–W3 devices).

Typical output spectra for the W1–W4 waveguide lasers are shown in Fig. 4 for the same $T_{OC} = 9\%$. For the W1, W3, and W4 waveguide devices, laser oscillation occurred at ~1.84 μm and for the W2 laser, at a much longer wavelength of ~1.92 μm. This spectral behavior is in agreement with the gain spectra of Tm^{3+} in KLuW for light polarization $E\|N_m$, because an increase of the inversion ratio (caused by an increase in the intracavity losses for the same T_{OC}) leads to the appearance of local maxima in the spectra at ~1.94, 1.92, and 1.84 μm [13]. As a consequence, the W2 waveguide provides lower losses, which agrees with Fig. 3(a).

The far-field intensity profiles of the laser mode were captured using a FIND-R-SCOPE near-IR camera, Fig. 5. The profiles are slightly elliptical due to the asymmetry of the stress field within the cladding measured by micro-Raman analysis, Fig. 2(a).

The PQS regime of the fs-DLW Tm:KLuW waveguide laser was realized using the waveguide W2 with the lowest cavity loss and a transmission-type SWCNT-based SA. Purified arc-discharge SWCNTs were used. The SWCNT/PMMA film (thickness: ~300 nm) was spin-coated onto an uncoated ~1 mm thick quartz substrate [19]. The individual SWCNTs were well distributed in the film and randomly oriented (spaghetti-like). The transmission spectrum of the SA contains a broad absorption band spanning from ~1.6 to 2.3 μm. It is related to the first fundamental transition of semiconducting carbon nanotubes (E_{11}). The initial (small-signal) transmission of the SA at ~1.84 μm was 97.4%, the saturation intensity for nanosecond pulse duration $I_{sat} \sim 7$ MW/cm^2, and the saturable absorption $\alpha'_S = 0.55\%$ [22]. The SA was inserted between the waveguide and OC at a minimum separation. Two OCs ($T_{OC} = 5\%$ and 9%) were studied.

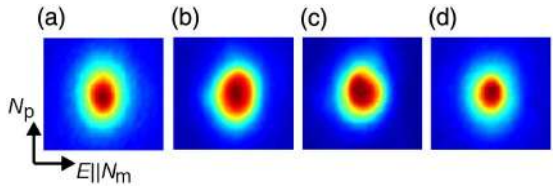

Fig. 5. Far-field intensity profiles of the CW laser mode of the fs-DLW Tm:KLuW waveguide lasers W1–W4 (a)–(d) (not in scale), at maximum P_{abs} according to Fig. 3(a).

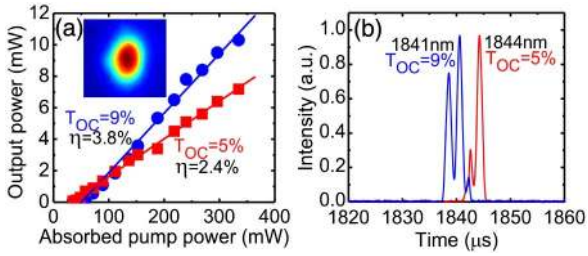

Fig. 6. SWCNT PQS fs-DLW Tm:KLuW waveguide laser: (a) input-output dependences, η-slope efficiency, inset: far-field profile of the laser mode; (b) typical laser emission spectra at $P_{abs} = 0.33$ W.

Stable passive Q-switching of the Tm:KLuW waveguide laser was achieved. The corresponding output characteristics are shown in Fig. 6(a). For $T_{OC} = 9\%$, the laser generated a maximum average output power of 10.3 mW at ~1841 nm corresponding to $\eta = 3.8\%$. The laser threshold was at $P_{abs} = 41$ mW and the conversion efficiency with respect to the CW mode η_{conv} was 22%. For $T_{OC} = 5\%$, 7.2 mW of average output power were achieved at 1844 nm. The spectra of the laser emission are shown in Fig. 6(b). The laser output was linearly polarized, $E\|N_m$.

The pulse characteristics, including the pulse duration (FWHM) $\Delta\tau$, pulse repetition frequency (PRF), pulse energy $E_{out} = P_{out}/\text{PRF}$, and peak power $P_{peak} = E_{out}/\Delta\tau$, are shown in Fig. 7. All of them are strongly dependent on P_{abs}, which is typical for "fast" SAs and related to the dependence of their bleaching on the pump power. It should be noted that close to the threshold, Q-switching was not very stable. Therefore only the P_{abs} range of 0.13…0.33 W was analyzed, Fig. 7. For $T_{OC} = 9\%$, $\Delta\tau$ shortened from 98 to 50 ns and E_{out} increased from 2.7 to 7.0 nJ. The PRF increased almost linearly from 1.0 to 1.48 MHz. The maximum P_{peak} reached 141 mW. For $T_{OC} = 5\%$, the best pulse characteristics were 4.7 nJ/42 ns at PRF = 1.54 MHz and P_{peak} was 110 mW. The pulse characteristics were numerically simulated with a model of a quasi-three level active material and a "fast" SA

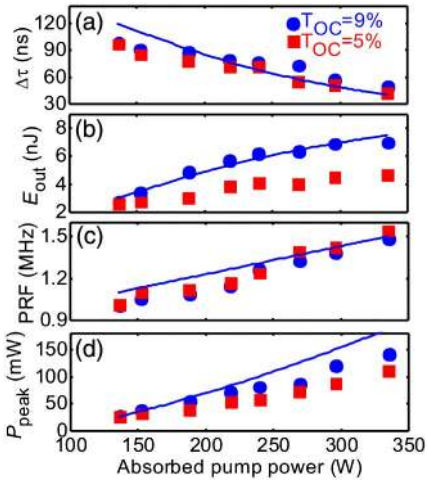

Fig. 7. SWCNT PQS fs-DLW Tm:KLuW waveguide laser: (a) pulse duration, $\Delta\tau$; (b) pulse energy, E_{out}; (c) pulse repetition frequency, PRF; and (d) peak power, P_{peak}. Blue curves—modeling for $T_{OC} = 9\%$.

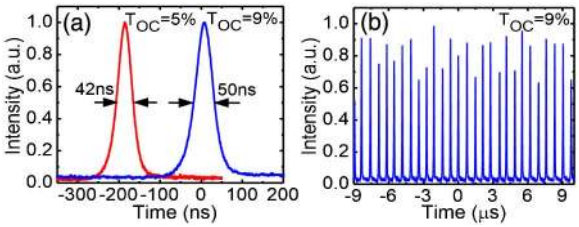

Fig. 8. SWCNT PQS fs-DLW Tm:KLuW waveguide laser: (a) oscilloscope traces of the shortest pulses; (b) the corresponding pulse train for $T_{OC} = 9\%$, $P_{abs} = 0.33$ W.

[22] for $T_{OC} = 9\%$, showing good agreement with the experiment (curves in Fig. 7).

The pulse duration ($\Delta\tau = 42$ ns) achieved in the present work is a record among all the PQS Tm waveguide lasers reported to date for both "fast" (graphene) and "slow" (Cr^{2+}:ZnSe) SAs. This short pulse duration is related to the use of a compact waveguide laser design (total geometrical cavity length: 4 mm) leading to a short cavity round-trip time, and a relatively small ratio of the non-saturable losses to the total absorption inherent to the SWCNT-SA ($\alpha'_S/\alpha' = 0.21$) and, hence, its higher modulation depth.

The typical oscilloscope traces of the output from the PQS fs-DLW Tm:KLuW waveguide laser are shown in Fig. 8. The single pulses had nearly Gaussian temporal shape. The intensity instabilities in the pulse train were <20% and the rms pulse-to-pulse timing jitter was <15%. The Q-switching instabilities are attributed to the heating of SA by residual pump [23].

The efficiency of the fs-DLW Tm:KLuW waveguide lasers can be improved by reducing the intracavity losses (by optimizing the DLW cladding waveguide structure, butt-coupling of the laser mirrors, or direct deposition of the SA on the face of the crystal), by increasing T_{OC}, or by increasing the Tm^{3+} doping level. The latter will lead to a stronger CR for Tm^{3+} ions [16] and increase the pump absorption while keeping a short cavity length. We emphasize the very high transition cross sections of Tm^{3+} in KLuW [13,15] allowing for high absorption and gain within very compact devices.

In conclusion, we report on the first fs-DLW waveguide lasers in Tm:DT crystals. Two types of waveguides were prepared: with circular or photonic-crystal-like cladding. A 3 at. % Tm:KLuW crystal was used as an active material and continuous-wave and passively Q-switched lasing at ~2 μm was demonstrated. CW lasing was observed for both types of waveguides. The best performance was obtained with the waveguide laser containing a circular cladding, with 46 mW at 1912 nm. In the PQS mode, using SWCNTs as the SA, 7 nJ/50 ns pulses were generated at a repetition frequency of ~1.5 MHz, representing the shortest pulses ever achieved in PQS Tm waveguide lasers. The presented waveguide preparation and lasing characteristics are very encouraging for DT waveguide lasers of this type doped with Tm^{3+} and Ho^{3+}.

Funding. Ministerio de Economía y Competitividad (MINECO) (FIS2013-44174-P, FIS2015-71933-REDT, MAT2013-47395-C4-4-R, MAT2016-75716-C2-1-R, TEC 2014-55948-R); Departament d'Innovació, Universitats i Empresa, Generalitat de Catalunya (DIUE) (2014SGR1358); Junta de Castilla y León (UIC016, SA046U16); Institució Catalana de Recerca i Estudis Avançats (ICREA) Academia (2010ICREA-02); H2020 Marie Skłodowska-Curie Actions (MSCA) (657630); Government of the Russian Federation (074-U01); National Research Foundation of Korea (NRF) Korea of MSIP (2016R1A2A1A05005381).

Acknowledgment. F. D. acknowledges additional support through the ICREA academia for excellence in research. X. M. acknowledges support from the European Union's Horizon 2020 research and innovation programme under the Marie Skłodowska-Curie. P. L. acknowledges financial support from the Government of the Russian Federation through the ITMO Post-Doctoral Fellowship scheme. S. Y. C. and F. R. acknowledge financial support from NRF Korea of MSIP.

REFERENCES

1. S. Taccheo, G. D. Valle, R. Osellame, G. Cerullo, N. Chiodo, P. Laporta, O. Svelto, A. Killi, U. Morgner, M. Lederer, and D. Kopf, Opt. Lett. **29**, 2626 (2004).
2. K. M. Davis, K. Miura, N. Sugimoto, and K. Hirao, Opt. Lett. **21**, 1729 (1996).
3. M. Ams, G. D. Marshall, P. Dekker, J. A. Piper, and M. J. Withford, Laser Photon. Rev. **3**, 535 (2009).
4. J. Siebenmorgen, T. Calmano, K. Petermann, and G. Huber, Opt. Express **18**, 16035 (2010).
5. T. Calmano, J. Siebenmorgen, A.-G. Paschke, C. Fiebig, K. Paschke, G. Erbert, K. Petermann, and G. Huber, Opt. Mater. Express **1**, 428 (2011).
6. G. A. Torchia, A. Rodenas, A. Benayas, E. Cantelar, L. Roso, and D. Jaque, Appl. Phys. Lett. **92**, 111103 (2008).
7. T. Calmano, J. Siebenmorgen, O. Hellmig, K. Petermann, and G. Huber, Appl. Phys. B **100**, 131 (2010).
8. Y. Tan, A. Rodenas, F. Chen, R. R. Thomson, A. K. Kar, D. Jaque, and Q. Lu, Opt. Express **18**, 24994 (2010).
9. A. Ródenas, G. Zhou, D. Jaque, and M. Gu, Appl. Phys. Lett. **93**, 151104 (2008).
10. D. G. Lancaster, S. Gross, H. Ebendorff-Heidepriem, K. Kuan, T. M. Monro, M. Ams, A. Fuerbach, and M. J. Withford, Opt. Lett. **36**, 1587 (2011).
11. D. G. Lancaster, S. Gross, A. Fuerbach, H. Ebendorff-Heidepriem, T. M. Monro, and M. J. Withford, Opt. Express **20**, 27503 (2012).
12. Y. Ren, G. Brown, A. Ródenas, S. Beecher, F. Chen, and A. K. Kar, Opt. Lett. **37**, 3339 (2012).
13. V. Petrov, M. C. Pujol, X. Mateos, Ò. Silvestre, S. Rivier, M. Aguiló, R. Solé, J. Liu, U. Griebner, and F. Díaz, Laser Photon. Rev. **1**, 179 (2007).
14. M. Pollnau, Y. E. Romanyuk, F. Gardillou, C. N. Borca, U. Griebner, S. Rivier, and V. Petrov, IEEE J. Sel. Top. Quantum Electron **13**, 661 (2007).
15. O. Silvestre, M. C. Pujol, M. Rico, F. Güell, M. Aguiló, and F. Díaz, Appl. Phys. B **87**, 707 (2007).
16. K. van Dalfsen, S. Aravazhi, C. Grivas, S. M. García-Blanco, and M. Pollnau, Opt. Lett. **37**, 887 (2012).
17. J. M. Serres, X. Mateos, P. Loiko, K. Yumashev, N. Kuleshov, V. Petrov, U. Griebner, M. Aguiló, and F. Díaz, Opt. Lett. **39**, 4247 (2014).
18. F. M. Bain, A. A. Lagatsky, R. R. Thomson, N. D. Psaila, N. V. Kuleshov, A. K. Kar, W. Sibbett, and C. T. A. Brown, Opt. Express **17**, 22417 (2009).
19. W. B. Cho, J. H. Yim, S. Y. Choi, S. Lee, A. Schmidt, G. Steinmeyer, U. Griebner, V. Petrov, D.-I. Yeom, K. Kim, and F. Rotermund, Adv. Funct. Mater. **20**, 1937 (2010).
20. P. Loiko, X. Mateos, S. Y. Choi, F. Rotermund, J. M. Serres, M. Aguiló, F. Díaz, K. Yumashev, U. Griebner, and V. Petrov, J. Opt. Soc. Am. B **33**, D19 (2016).
21. H.-D. Nguyen, A. Ródenas, J. R. V. de Aldana, J. Martínez, F. Chen, M. Aguiló, M. C. Pujol, and F. Díaz, Opt. Express **24**, 7777 (2016).
22. R. Lan, P. Loiko, X. Mateos, Y. Wang, J. Li, Y. Pan, S. Y. Choi, M. H. Kim, F. Rotermund, A. Yasukevich, K. Yumashev, U. Griebner, and V. Petrov, Appl. Opt. **55**, 4877 (2016).
23. J. M. Serres, P. Loiko, X. Mateos, K. Yumashev, U. Griebner, V. Petrov, M. Aguiló, and F. Díaz, Opt. Express **23**, 14108 (2015).